Pergamon

Journal of Structural Geology, Vol. 20, No. 2/3, pp. 149 to 162, 1998

0191-8141/98 $19.00 + 0.00

PII: S0191-8141(97)00073-4

Strain localisation and incremental deformation within ice masses, Framnes Mountains, east Antarctica

BRETT A. MARMO and CHRISTOPHER J. L. WILSON

School of Earth Sciences, The University of Melbourne, Parkville, Victoria, 3052, Australia

(*Received* 3 *January* 1997; *accepted in revised form* 9 *September* 1997)

Abstract—Mesoscale fracture analysis of brittle features has been used to identify zones of localised ductile deformation within an ice stream, moving at $\sim 20\ ma^{-1}$ in the Framnes Mountains, east Antarctica. Ground-based survey of three strain grids has been integrated with the detailed structural analysis to develop a model of temporal and spatial variation in strain localisation within large high strain zones. Modelled strain distributions are in good agreement with the occurrence and sense of movement across zones of high ductile strain which have been inferred from observed brittle features. The major zone of high strain is 3 km wide and 15 km long and deformed dextrally at a strain rate of $6.17 \times 10^{-3}\ a^{-1}$ over the two year period of observation. Despite this constant annual strain rate the internal deformation was incremental, localised and temporal in nature resulting in the development of new zones of fracturing. © 1998 Published by Elsevier Science Ltd.

INTRODUCTION

Polar glaciers provide an ideal medium to study the variation of strain with respect to time and space and the way in which this affects the geometries of both brittle and ductile features developed within high strain zones. A better understanding of the conditions which give rise to the progressive change in an ice mass containing a shear zone system will shed light on our understanding of the mechanics and kinematics of deformation and provide a good framework for interpretation of these structures (Hudleston, 1980; Sharp *et al.*, 1988; Lawson *et al.*, 1994). As ice laboratory experiments (Schulson *et al.*, 1984; Rist *et al.*, 1988) have not yet reproduced the conditions experienced in the field, there are no reliable fracture theories of ice to predict the onset of crevassing. The aim here is to take a phenomenological approach by analysing the association between the presence (or absence) of fractures and the measured strain rate. It will be shown that field-based structural analysis of brittle features has identified several zones of localised ductile deformation in the outlet glaciers that flow through the Framnes Mountains, MacRobertsons Land, east Antarctica. Strain analysis has revealed that while a shear zone deforms at a constant rate, internally the deformation is incremental as a result of spatial variations of the strain rate.

Previous field studies of shear zones in ice masses either describe localised ductile phenomena in order to generalise strain conditions (Hambrey, 1977; Hudleston, 1976, 1980; Whillians *et al.*, 1987) or have attempted to relate the formation of crevasses by analysis of the exact conditions under which they occur (Holdsworth, 1969; Kehle, 1964; Sharp *et al.*, 1988). Kehle (1964) explored analogues between the failure of ice and rock and makes the central assumption that crevasses are fractures formed once a critical condition of stress or strain rate is reached in the surface layers of an ice mass. This is similar to the approach taken by Vaughan (1993) who makes stress predictions based on the strain field within the ice sheet. In the approach that we adopt in this paper we can relate structural elements to ice velocity and relate them over time. We also compare our surface strain measurements to local dilatations that are occurring in the ice mass.

The glacial system studied comprises three, nearly parallel, outlet glaciers that cover approximately $2400\ km^2$ and are calving into Holme Bay within 100 m of the grounding line (Fig. 1). The distinctive surface morphology of active flowing ice is visible as abundant crevasses at the surface, and long curvilinear flow bands (Fig. 1). Ground-based surveys of five strain grids monitored the ice movement from December 1993 to January 1995, and from January 1995 to January 1996. These provide two sets of displacement vectors referred hereafter as Year 1 and Year 2, respectively. The strain grids are located 15 km up-stream from the grounding line, at which the ground ice sheet begins to float. The survey has concentrated on Ice Stream B which is the central of the three and is bounded by the Masson and David Ranges. Ice Stream B flows at approximately $20\ ma^{-1}$ with a maximum recorded flow of $21.8\ ma^{-1}$ and a minimum flow $11.3\ ma^{-1}$. Ablation in the area studied was between $150\ mm\ a^{-1}$ and $350\ mm\ a^{-1}$. Previously Kizaki (1969a,b) studied the Framnes Mountains glacial system and focused on the Mawson Station area. Marmo and Dawson (1996) published initial structural observations in the outlet glacier and ice flow data for Ice Stream B and Ice Stream C (Fig. 1).

STRUCTURAL ELEMENTS

Within the blue ice exposed in the ablation zone, there are two prominent foliations. Interleaved sub-vertical layers of dark and light blue ice define a foliation (S_1).

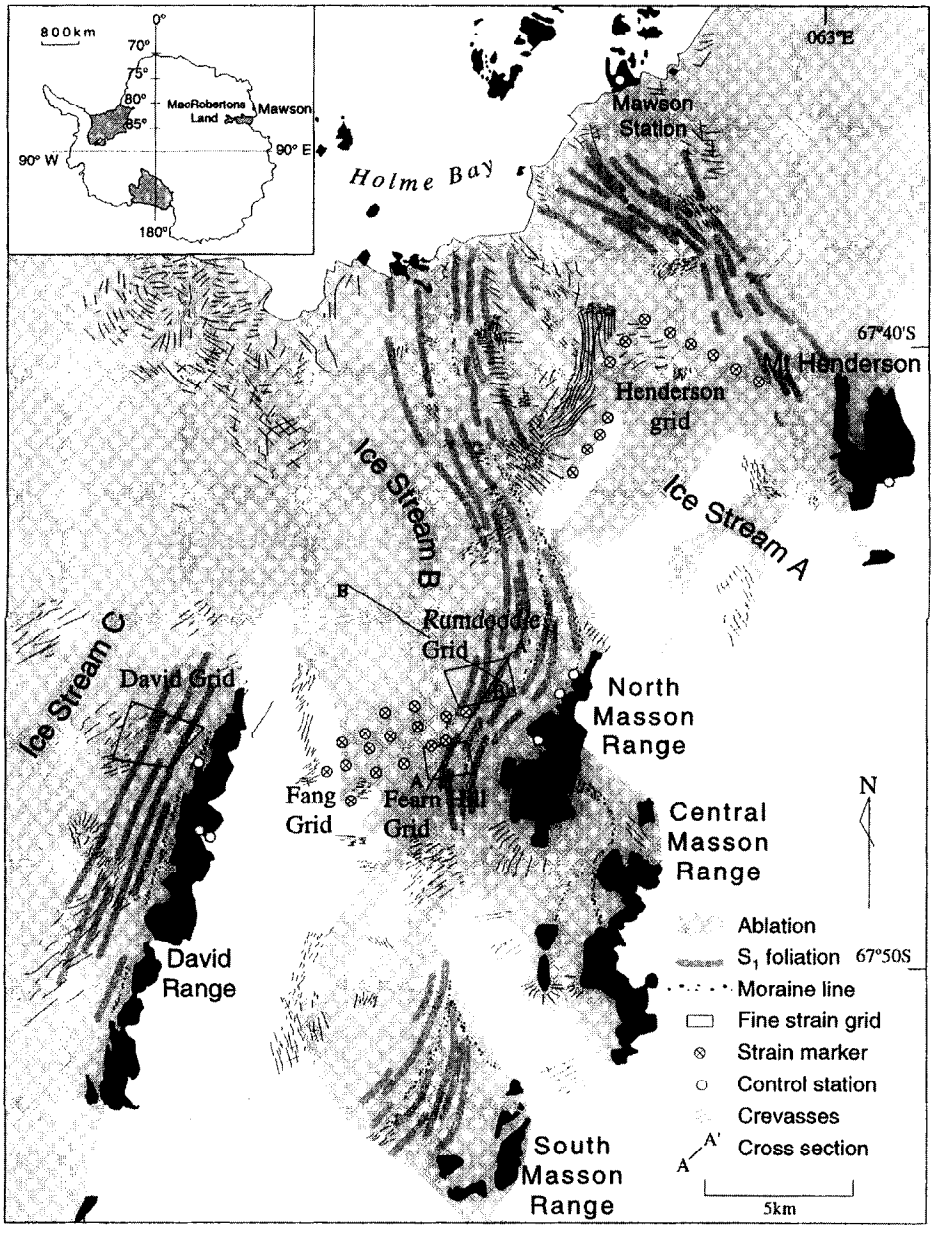

Fig. 1. Glacial system of the Framnes Mountains (black areas), MacRobertsons Land, have a strain marker spacing of 200 m–300 m. The individual strain markers of the Fang and Henderson grids have been included as have the localities of survey control stations including the permanent AUSLIG monument, AUS64 located at Mawson Station. Crevasse fields with crevasses wider than 100 mm are represented. The orientation of the S_1 foliation has been determined from aerial photographs. Inset: The Antarctic continent with the Mawson area shown.

The layers are hundreds of millimetres to tens of metres wide, with the largest ones observable on aerial photographs. The layers are defined by different bubble contents within coarse-grained ($\sim$5 mm) interlocking ice grain aggregates. The S_1 foliation has developed in regions of high shear strain adjacent to the mountain ranges. Heterogeneities within the accumulation zone becoming flattened and rotated by progressive simple shear to produce the foliation as described by Hooke and Hudleston (1978). The Rumdoodle and Fearn Hill grids have been positioned in areas where the S_1 foliation has been recognised, in order to monitor a zone with high shear strain. The orientation of the foliation is parallel to the velocity vectors determined from these two grids.

A second foliation (S_2) locally overprints the S_1 foliation. It is defined by fine layers of bubbles less than 1 mm wide which have formed as a result of annealing of fractures or closure of small fractures. The S_2 foliation has not been recognised in the Rumdoodle grid but has been observed in the northern part of the Fearn Hill grid. Fine fractures in the southern section of the Fearn Hill grid may have been passively transported north and become annealed.

Widespread tensional fracturing occurs throughout

the glacial system with surface fractures that vary in width from 2 mm to 5 m. In the Rumdoodle and Fearn Hill grids, crevasses do not exceed 0.1 m in width, and most commonly range between 5 mm and 50 mm. The fracture density varies from 0.1 to 3 fractures per metre. Open fractures may become filled with snow and/or water that becomes frozen in the appropriate weather conditions to produce crevasse traces (Hambrey and Milnes, 1977). In the Rumdoodle and Fearn Hill grid areas the fractures are not wide, and rapidly fill with surface melt water during mid-afternoon, and freeze during the evening. Depending on climatic conditions, the open fractures generally freeze within a week of opening if they do not continue to dilate. Open fractures therefore imitate the immediate stress regime and are not necessarily indicative of the long term strain history.

Crevasse traces occur as coarse-grained, translucent columnar ice, commonly with a median suture composed of a well defined plane of bubbles midway between the walls of the fracture. They appear distinctly different to the bubbly blue ice that hosts the traces. Crevasse traces by nature are relics of crevasses and are a representation of palaeo-stress regimes where the σ_1 (major principal compressive stress direction) is contained within the trend of the trace. Traces may be re-orientated by rigid body rotation while they are passively transported; however the relationship between the trace and the S_1 foliation remains constant. Initially the crevasse trace orientation is highly variable with changes up to 90° over a scale of metres, mimicking the surface expression of open crevasses (Fig. 2). These occur as arrays of en échelon fractures, similar to those described in rocks by Gamond (1987). Exhumation of the crevasse traces, by ablation, reveals that the fractures are generally planar at depth. Crevasse traces that are several years old and that have been exhumed to the surface of the glacier, generally have a linear surface expression.

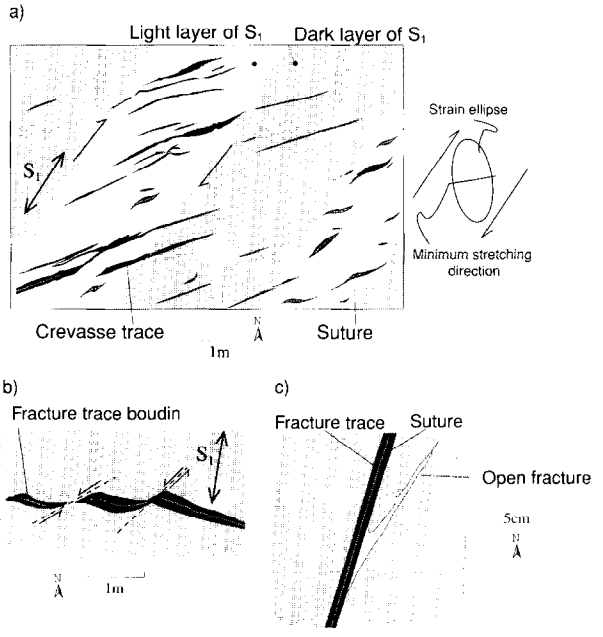

Fig. 2. Typical fracture patterns observed in the ice mass. (a) Field sketch from the eastern margin of the Rumdoodle grid showing en échelon fracturing oblique to S_1 due to dextral shearing. Straight or planar fractures parallel the minimum extension direction of the finite strain ellipse. En échelon fractures are concentrated in the light layers (weakened by bubbles). (b) Boudinaged fracture trace. A refrozen fracture has been passively transported into a region were the extension direction is sub-parallel to the orientation of the trace. Sinistral shear is indicated by the offset of boudins. (c) Field sketch of an open fracture that has initiated on the margin of a fracture trace. The new fracture is oblique to the old trace and is probably related to a change in stress regime or because the trace was formed up-stream and has then been passively transported in a different stress regime. It is believed the former is the most likely scenario.

SHEAR SENSE CRITERIA

The geometry of fractures and their relationship to the S_1 foliation can be used to determine shear sense (Marmo and Dawson, 1996). In regions undergoing deformation, with a component of simple shear, en échelon style fracturing occurs oblique to the S_1 foliation. In a dextral regime, extensional en échelon fractures make an acute clockwise angle with S_1 and in a sinistral regime, an acute anti-clockwise angle (Fig. 2a). The degree of rotation away from S_1 foliation is dependent on the component of pure shear. Passive transportation of pre-existing crevasse traces into areas experiencing brittle deformation can result in the offset of the crevasse traces by younger crevasses. The relative offset also provides a shear sense indicator.

Boudinage of thick crevasse traces (> 100 mm) has occurred after the traces were passively transported into extensional environments. The relative position of the boudins can be used to indicate sense of shear. It is necessary to distinguish between boudins that have been laterally offset without rotating, and boudins that have been back-rotated *in situ*, as these will give opposite kinematic indications (Hanmer and Passchier, 1991). The orientation of intact crevasse traces up-stream represents the initial orientation of boudinaged traces. Assessment of the amount and direction of rotation is possible by measuring the orientation of crevasse traces up-stream before they become boudinaged.

STRUCTURAL INTERPRETATIONS

Shear sense criteria based on brittle geometry imply that macroscale zones of localised ductile shear strain exist within the ice mass (Marmo and Dawson, 1996) (Fig. 3). The zones of localised strain are kilometres long, hundreds of metres wide and are separated by areas that are fracture free. Beginning between the North Masson and David Ranges and extending tens of kilometres north are three dextral shear zones that are responsible for incremental increases in flow rate to the west. The Rumdoodle grid lies close to the centre of the most easterly of these high strain zones. Between the Central

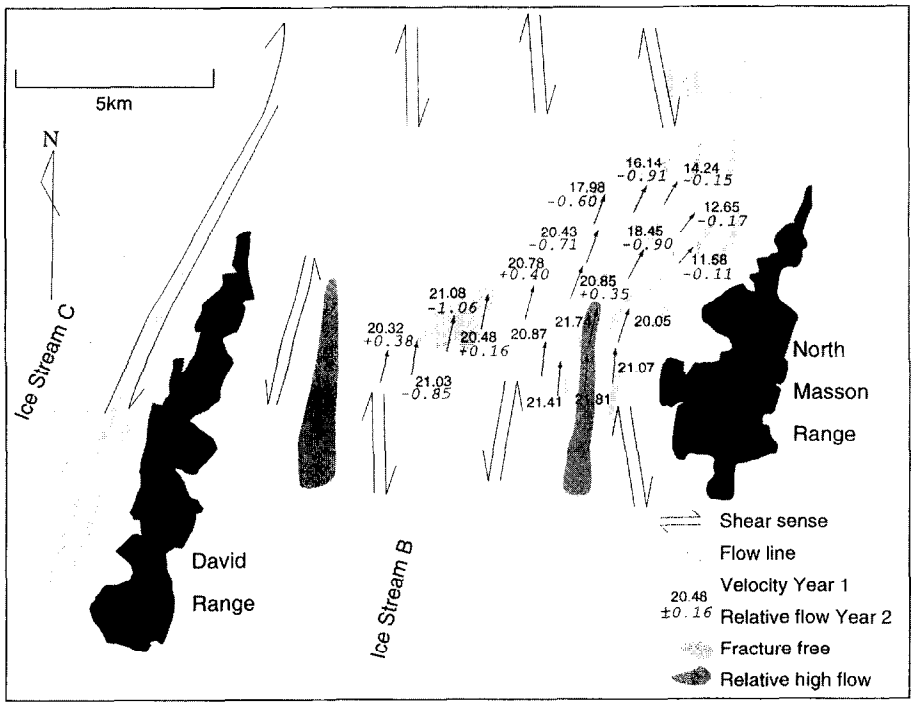

Fig. 3. Distribution of shear zones in Ice Stream B and Ice Stream C inferred from field based structural analysis. In the northern section of Ice Stream B there are three dextral shear zones separated by unfractured ice. The Rumdoodle and Fearn Hill strain grids monitor the eastern shear zones. Between the David and North Masson Ranges are two sinistral shear zones and two dextral shear zones, that produce two relative high flow areas and a centrally located fracture free low flow zone. A summary of the local ice flow data has also been included. The velocity calculated during Year 1 is shown with the relative change in velocity (±) during Year 2. Note that the calculated velocity vectors are parallel to S_1 foliation and correlate with the inferred structural features.

Masson and David Ranges is a zone of sinistral shear between two zones of dextral shear, indicating that there are at least two streams of relatively high flow rate, one close to the David Range, and a second, 3 km west of the southern extent of the North Masson Range. The latter of these relatively high flow regions extends through the centre of the Fearn Hill grid.

Brittle structures observed in the Rumdoodle grid

During Year 1 a broad zone of open crevasses ranging in width from 5 mm to 50 mm extended from the SW corner and eastern margin of the Rumdoodle grid to the NE corner. The orientation of the open crevasses gradually rotated from 022° in the west to 045° in the east (Fig. 4). All traces made an acute clockwise angle with the S_1 foliation indicating a dextral shear sense. Crevasse traces occur in a region slightly wider than that with open crevasses and range in width from 2 mm to 50 mm. In the western part of the Rumdoodle grid, open crevasses and crevasse traces offset older crevasses at an acute clockwise angle. Fracture traces are typically offset with a dextral sense of movement. Crevasse traces also provide sites for the initiation of fractures which propagate away from the initial trace at acute clockwise angles (Fig. 2b).

The broad zone of open crevasses recognised during Year 1 separated into two areas during Year 2. Two additional areas with open crevasses also appeared on the eastern margin of the Rumdoodle Grid. During Year 2 crevasse traces occurred in the same area as was observed in Year 1, reflecting their enduring nature. The traces were concentrated in areas with open crevasses and in areas directly down stream due to passive transportation away from fracturing zones (Fig. 4). The maximum concentration of fracture traces was 3 m^{-2}. Features such as dextral offset of crevasse traces and initiation of crevasses from crevasse traces at low angles were again recognised.

Brittle structures observed in the Fearn Hill grid

Open fractures were observed only in the northeast corner of the Fearn Hill grid, both in Year 1 and Year 2. The open fractures were from 2 mm to 5 mm wide and oriented due north. Fracture traces are more extensive than within the Rumdoodle grid though not as highly concentrated (Fig. 4). Traces are generally from 2 mm to 10 mm wide except in the southwest corner where they are up to 100 mm wide. The highest concentration of fracture traces of 1.5 m^{-1} occurred in the centre of the grid. No open fractures were observed here, indicating that crevassing may have been occurring between observation seasons.

The orientation of fracture traces rotates clockwise from trending E–W to N–S moving from the southwest

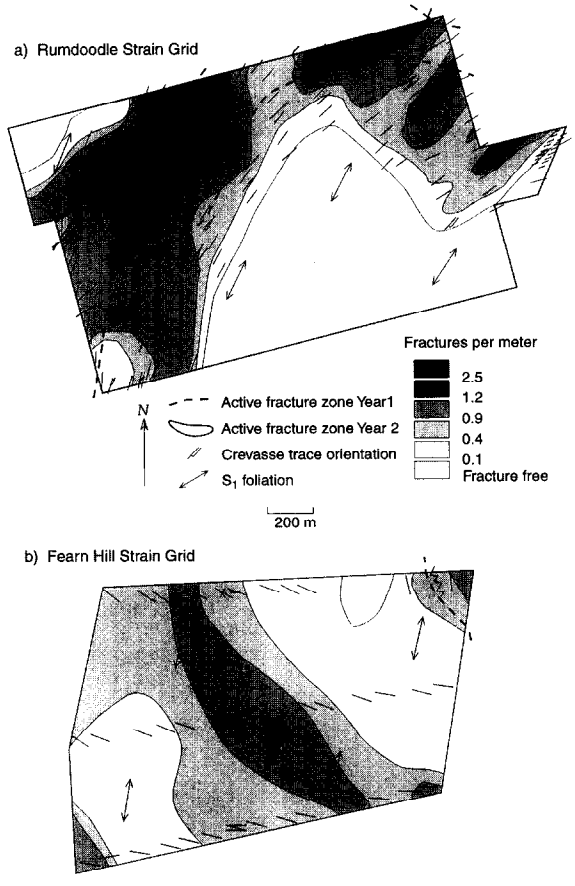

Fig. 4. Fracture distribution and concentration in strain grids. (a) In the Rumdoodle grid a single broad zone of open fractures developed during Year 1. During Year 2 four discrete zones of open fractures were recognised, two new areas appeared in the eastern portion of the grid and the single zone through the centre separated into a zone on the northern margin and another on the western margin. Fracture traces were concentrated around, and down-stream of the open fracture zones. (b) In the Fearn Hill grid, open fractures were observed only in the NE corner. Fracture traces were more extensive than in the Rumdoodle strain grid though not as concentrated. Only a 200 m wide area in the north of the grid lacked fracture traces.

corner of the grid to the northeast. All traces made an acute anti-clockwise angle with the S_1 foliation, indicating sinistral shear. The anti-clockwise rotation from S_1 indicates a variation from extensional flow in the SW to compressional flow in the NE. Fractures offset older fracture traces at low angles and indicate a sinistral sense of movement throughout the grid. In the central part of the northern margin of the grid a second set of fracture traces oriented 012° overprint the main set of fractures oriented 112°, though no sense of movement was evident. Offset of fracture trace boudins that originate 1 km upstream indicate a sinistral sense of shear (Fig. 2).

SURVEY METHODS

A glacial movement survey has been undertaken on the blue ice areas in order to integrate ice surface movement rates and ice fracture analysis. Strain markers consist of six metre long lengths of bamboo drilled one metre into the ice. In all, there are 160 strain markers divided into five strain grids located in Ice Streams A, B and C (Fig. 1). Detailed here are the results from the Rumdoodle, Fearn Hill and Fang strain grids in Ice Stream B (Fig. 1), as these best represent the uniform flow pattern of the three ice streams. The Rumdoodle and Fang grids are situated on a relatively flat surface so that topography has little effect on flow or the development of the structural features. The Fearn Hill grid is situated on an ice wave (Fig. 5a) so that the structural development can be compared to that of the Rumdoodle grid. Ice radar data have been used to calculate the ice depth in these areas (Fig. 5), providing knowledge of another boundary that may affect structures in the surface layer of the ice. Ice depth varies between 450 m and 750 m in the region surveyed with vertical fluctuations of 100 m that occur over kilometres. Below the Rumdoodle Grid is a valley and several small peaks occur in the bedrock below the Fang grid (Fig. 5b).

The Rumdoodle and Fearn Hill strain grids are fine grids with a grid spacing from 200 m to 300 m. These were positioned in areas of high shear strain identified from aerial photographs. The Fang grid is a line grid with a grid spacing between 700 m and 1000 m. The Fang grid was constructed to monitor the overall flow rate of Ice Stream B and to detect any variation of flow. Both conventional survey techniques and differential GPS methods were utilised to measure the positions of strain markers during the 1993–4, 1994–5 and 1995–6 austral summers. To provide a permanent reference, seven survey control stations have been established in the surrounding bedrock. Each station consists of a 20 mm diameter steel rod drilled to a depth of 200 mm. Three stations are located in the David Range, three in the North Masson Range and another in the Mt Henderson area (Fig. 1). In addition, all measurements were adjusted with reference to the permanent Australian Surveying & Land Information Group (AUSLIG) monument, AUS64, located at Mawson.

Two single frequency Ashtech M-XII receivers and a single frequency Ashtech MS-XII receiver measured the majority of the surveys. Strain markers were surveyed with observation sessions generally ranging from 1.8×10^3 s to 6.0×10^4 s, over distances from 1 to 20 km. The length of the baseline and the satellite geometry dictated the length of the observation period. GPS baselines between survey control stations were measured using observation periods of from 3.6×10^3 s to 1.08×10^4 s over distances from 3 to 20 km. All conventional and GPS measurements have been processed using a Least Squares Adjustment technique, with the standard deviations of each coordinate being within 10 mm. The maximum calculation error in the position of each strain marker is within 50 mm. The maximum standard deviation for all displacement vectors is 100 mm and 0°15′.

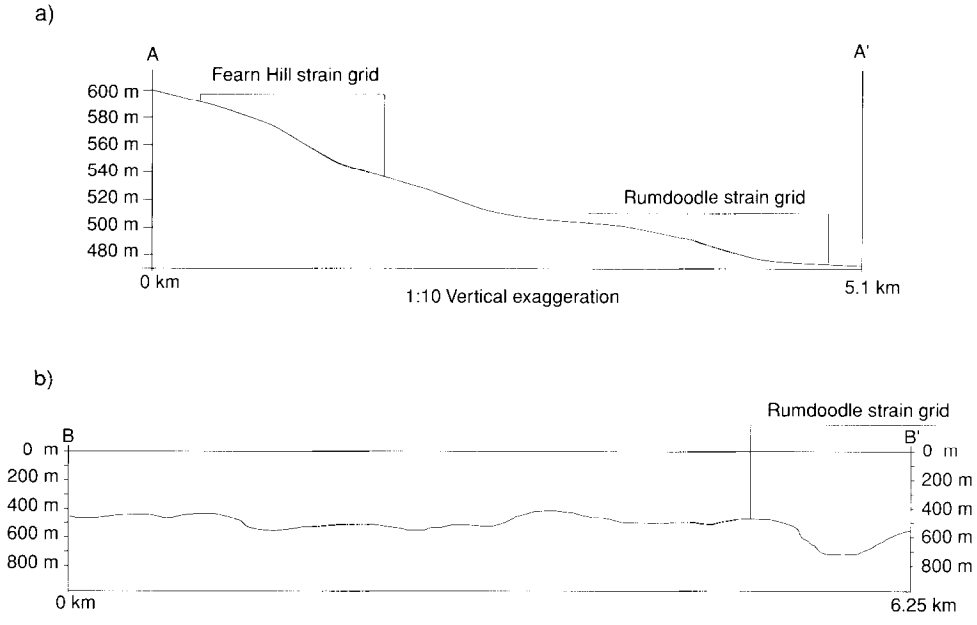

Fig. 5. Ice topography and bed-rock characteristics. (a) A vertical profile of ice surface in metres above sea level parallel to flow from south of the Fearn Hill grid (Fig. 1) to north of the Rumdoodle grid (A–A') with a vertical exaggeration of 1:10. The position of the Rumdoodle and Fearn Hill grids are shown. (b) Ice thickness in metres below the ice surface from ice radar data of a section perpendicular to flow (B–B'). The diagram is to true vertical scale. Locations of profiles A–A' and B–B' are shown on Fig. 1.

ICE VELOCITY

Markers in the Rumdoodle and Fang strain grids have been measured during all three summers, providing two sets of displacements. The strain markers in the Fearn Hill grid were measured twice in the 1994–5 summer with an interval of 35 days, and then measured again in the 1995–6 summer. All displacement measurements have been converted to velocity vectors with units of ma^{-1} as used by the glaciological community (Paterson, 1994). The maximum velocity recorded in Ice Stream B was 21.8 ma^{-1} from markers on the western side of the Fearn Hill grid, and the minimum velocity was 11.3 ma^{-1} from markers on the eastern side of the Rumdoodle grid. The results have been summarised in Fig. 3, and represent a slower moving glacial system (Paterson, 1994).

Ice Stream B moved on average between 0.2 ± 0.02 ma^{-1} and 1.0 ± 0.03 ma^{-1} slower during the second year across the 10 km width surveyed. However, a 2.5 km wide section in the centre of the ice stream moved between 0.16 ± 0.02 ma^{-1} and 0.40 ± 0.05 ma^{-1} faster during the second year. The western extremity of the Fang grid increased in velocity by 0.38 ± 0.03 ma^{-1}. There is no surface elevation evident for such variation in the flow rate such as the interstream ridges described by Whillians *et al.* (1987).

The Fearn Hill grid recorded a seasonal variation. The summer velocity was on average 0.16 ± 0.03 ma^{-1} higher than that recorded throughout the following year. The distribution of relative movement was not uniform, with markers in the centre moving between 0.10 ± 0.03 ma^{-1} and 0.40 ± 0.04 ma^{-1} faster during the summer, and markers to the west of the centre, and in the NE corner of the grid, moving between 0.06 ± 0.03 ma^{-1} and 0.28 ± 0.04 ma^{-1} slower during the summer period (Fig. 3).

STRAIN ANALYSIS

Displacement of each strain marker has been standardised to movement over 365 days. The two dimensional deformation analysis program 'Marker Analysis' (Bons *et al.*, 1993) was used to analyse quantitatively the kinematics of the deformation. Displacement vectors from markers have been resolved onto a horizontal datum in order to analyse the strain.

Strain analysis for Ice Stream B has been performed by compiling the data from the Fearn Hill, Rumdoodle and Fang grids. The maximum strain was recorded by the Rumdoodle grid. The region west of the Rumdoodle grid is undergoing relatively little deformation with a strain ratio less than between 1.001 and 1.003.

Both positive and negative shear strain rate values reflect a change from a dextral sense of shear in the east to sinistral in the west. The maximum shear strain rate of 7.26×10^{-3} was recorded in an area undergoing dextral shear by the Rumdoodle grid. The maximum sinistral value of 2.74×10^{-3} was recorded in the western section of the Fang grid. The sinistral and dextral areas were separated by a 1 km wide zone deforming without a component of simple shear (Fig. 6).

The orientation of the major principal axes of strain ellipses varies from a north-westerly trend on the eastern

margin of the surveyed area to a north-easterly trend on the western margin (Fig. 6). This rotation is partially due to a lateral change in flow direction. On the eastern margin the orientation of flow is towards north-northeast and on the western margin it is towards due north. A more important factor in the variation of strain orientation is deformation style. In the centre of the surveyed area the orientation of the major axis was orthogonal to the flow direction indicating that the ice is undergoing compressional flow (Nye, 1952). In the eastern region of the survey the major axes of the strain ellipse make an acute anti-clockwise angle from the S_1 foliation indicating a dextral shear sense. On the western margin, the major axes make a small acute clockwise angle from the flow direction indicating sinistral shear in an environment undergoing extension parallel to flow.

Annual strain variation in the Rumdoodle grid

The Rumdoodle grid recorded an insignificant increase in shear strain rate during the second year of the survey. The change was from $6.17 \times 10^{-3}\ a^{-1}$ during Year 1 to $6.18 \times 10^{-3}\ a^{-1}$ in Year 2. However, the nature and localisation of the deformation varied with time.

During Year 1 finite strain ratios varied from 1.003 to 1.010 with maximum values in the central area of the northern margin of the grid, and minimum values in the south eastern corner (Fig. 7). Shear strain rate within the grid varied from $9.78 \times 10^{-4}\ a^{-1}$ to $1.19 \times 10^{-3}\ a^{-1}$. All shear strain values are positive indicating a dextral component of simple shear throughout the studied area. Finite dilatation both greater than 1, indicating surface area increase, and less than 1, indicating surface area decrease, was detected. A broad area through the centre of the grid had finite dilatation values less than 1 with a minimum value of $0.978\ a^{-1}$ at the centre of the grid's southern margin. Surrounding this region and extending to the western, northern and eastern margins of the grid was a region of surface area increase, with a maximum dilatation rate of $1.003\ a^{-1}$. The orientation of the major axes of the strain ellipse rotates clockwise from 110° to 156° moving from west to east. This rotation reflects both the increase in dextral shear strain eastward and the lateral change in flow direction.

Strain markers recorded the same bulk shear strain across the Rumdoodle grid during the second year. However, the strain was localised into smaller areas, resulting in higher maximum and lower minimum values than those recorded during Year 1. The strain grid recorded the maximum finite strain ratio value 1.011 on the eastern margin of the grid, reflecting an overall eastward propagation of strain during Year 2 (Fig. 7). The grid recorded the minimum finite strain value of 1.001 in the south eastern corner and in the previously highly-strained centre. The variation of shear strain rate within the grid was also greater than that recorded in Year 1. The shear strain rate varied from $4.55 \times 10^{-4}\ a^{-1}$ and $9.67 \times 10^{-3}\ a^{-1}$.

The increase in shear strain was accompanied by clockwise rotation of the strain ellipses during Year 2 that was generally between 1° and 4° (Fig. 8). In localised pockets, such as the central northern region and north-east corner, the rotation was as high as 20° (Fig. 8). In the southeast corner, pure shear became more important, resulting in an anti-clockwise rotation of the strain ellipse of up to 4°.

Seasonal strain variation in the Fearn Hill grid

The seasonal velocity variation observed in the Fearn Hill grid accompanied a strong variation in strain rate and deformation style. During the 1994–5 summer, strain ratio varied between $1.000\ a^{-1}$ and $1.007\ a^{-1}$ with maximum values in the southern portion of the grid, and minimum values in the northwest (Fig. 9). The strain was strongly localised into several small zones, from 50 to 100 m wide. The majority of the Fearn Hill grid underwent sinistral shear, whilst an area in the northeast and another in the northwest deformed with a dextral shear sense. The maximum shear strain rate in the area which underwent sinistral deformation was $-5.91 \times 10^{-3}\ a^{-1}$. In the area that was deformed by dextral shear the maximum shear strain rate was $2.71 \times 10^{-3}\ a^{-1}$. Regions undergoing surface area increase were spread throughout the grid with maximum dilatation values of $1.005\ a^{-1}$. An area on the eastern margin of the grid recorded the maximum surface area decrease, with a dilatation rate of $0.996\ a^{-1}$. Other regions undergoing surface area decrease were also distributed about the Fearn Hill grid.

The orientation of the principal axes of the strain ellipse became highly variable during the 1994–5 summer, reflecting the partitioning of strain between different deformation regimes (Fig. 8). In the areas that were deformed with a component of sinistral shear, the major axes of the strain ellipse were oriented between 030° and 079° (Fig. 8). In the regions that underwent dextral shear, the area in the northeast corner of the grid had the long axes oriented at 104° and the area in the northwest had major axes at 132°. In the areas that had little or no shear strain, the major axes of the strain ellipse were perpendicular to the flow direction. This orientation indicates that pure shear deformed the regions in a compressional flow environment.

The strain rate in the Fearn Hill grid, from the period beginning in February 1995 to January 1996, displayed a 50% reduction. The strain grid recorded the maximum strain ratio value of $1.004\ a^{-1}$ in the northeast corner, and the minimum of $1.000\ a^{-1}$ in the southeast corner of the Fearn Hill grid (Fig. 9). Deformation was spread into broader zones than those observed during Summer 1994–5. This may be a function of either the increase in strain rate during summer or the different time scales over which the two displacements were measured. Discrete high strain zones may have been active during the winter but have been averaged over the 12 month measurements.

Fig. 6. Movement, topography and strain data from Ice Stream B. The data used for analysis was complied from the movements of the Fearn Hill, Fang and Rumdoodle strain grids during Year 2 (a) A summary of displacement data obtained using GPS survey techniques with vector lengths scale for velocity. Ice surface topography is included with the elevation in height above sea level in metres. (b) The distribution of calculated orientation of principal axes of the finite strain ellipse. The orientations correlate with the shear zones inferred from field observations. There is a west to east clockwise rotation of the major axes corresponding to a variation from a sinistral shear zone in the west, to a region of pure shear (E–W trend of axes) and finally to a dextral shear in the east. (c) Contours of shear strain rate. Positive values represent dextral shear sense and negative value represent sinistral shear. Zero values are in areas where pure shear dominates.

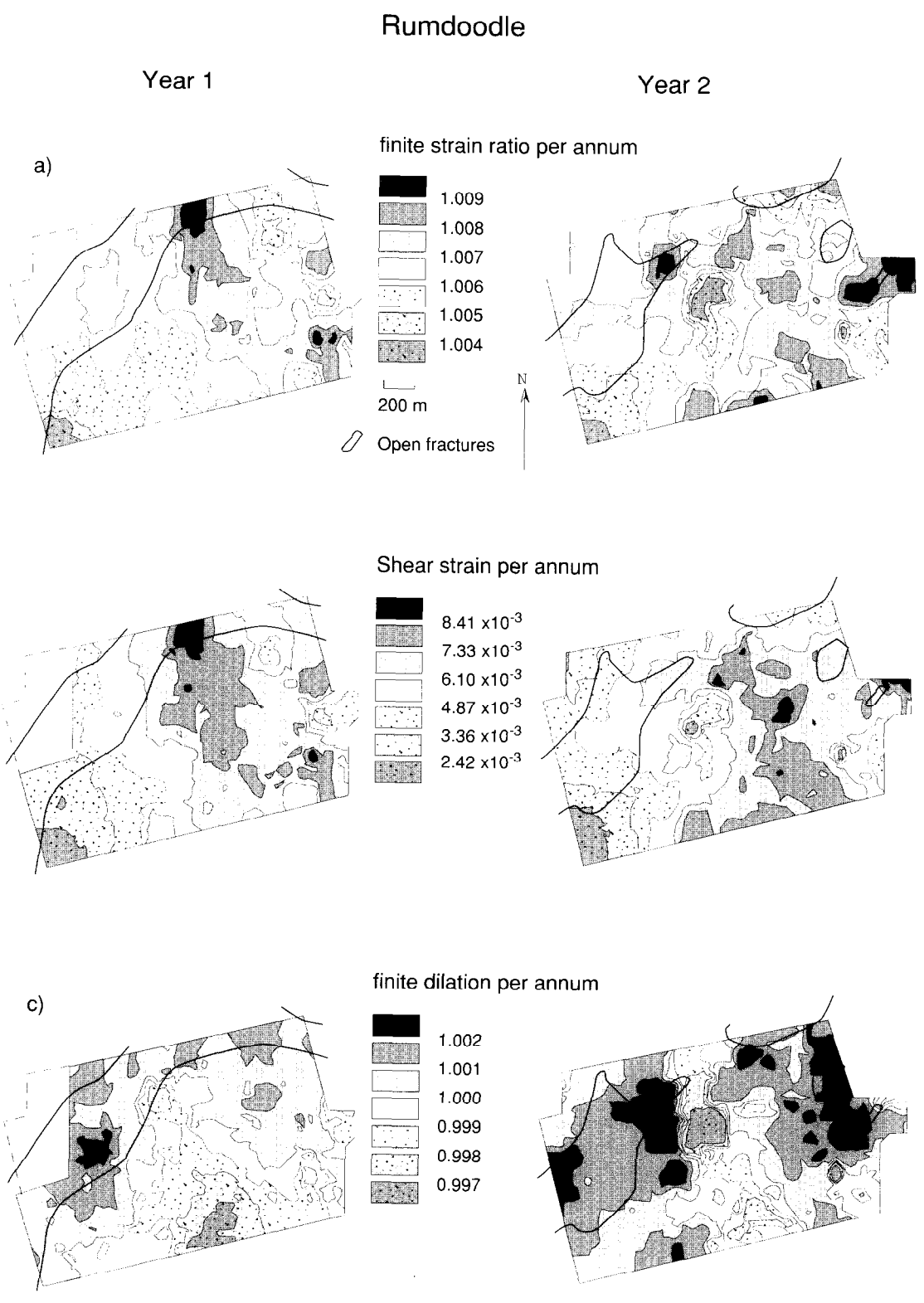

Fig. 7. Strain analysis of the Rumdoodle strain grid. The grid consists of 76 strain markers with a grid spacing of 200 m. Results from Year 1 (left) are compared to results from Year 2 (right). (a) A comparison of distribution of Year 1 vs Year 2 finite strain ratios. Strain propagated to the east of the grid during Year 2, with the maximum and minimum values partitioned into discrete areas during Year 2 producing an uneven strain distribution. The low strain area in the centre of the Year 2 grid had previously been relatively highly strained. (b) Distribution of shear strain rates. All values are positive indicating dextral shear sense. The maximum shear strain rate during Year 1 occurred through the centre of the strain grid. During Year 2 the shear strain was localised in the eastern part of the grid. (c) Dilatation rates. Values greater than 1 represent zones of increasing surface area, values less than 1 represent zones of decreasing surface area. The region of volume decrease in the centre of the grid during Year 1 propagated north during Year 2. Open fractures zone correlate with zone undergoing surface area increase, suggesting that crevassing is related to dilatation.

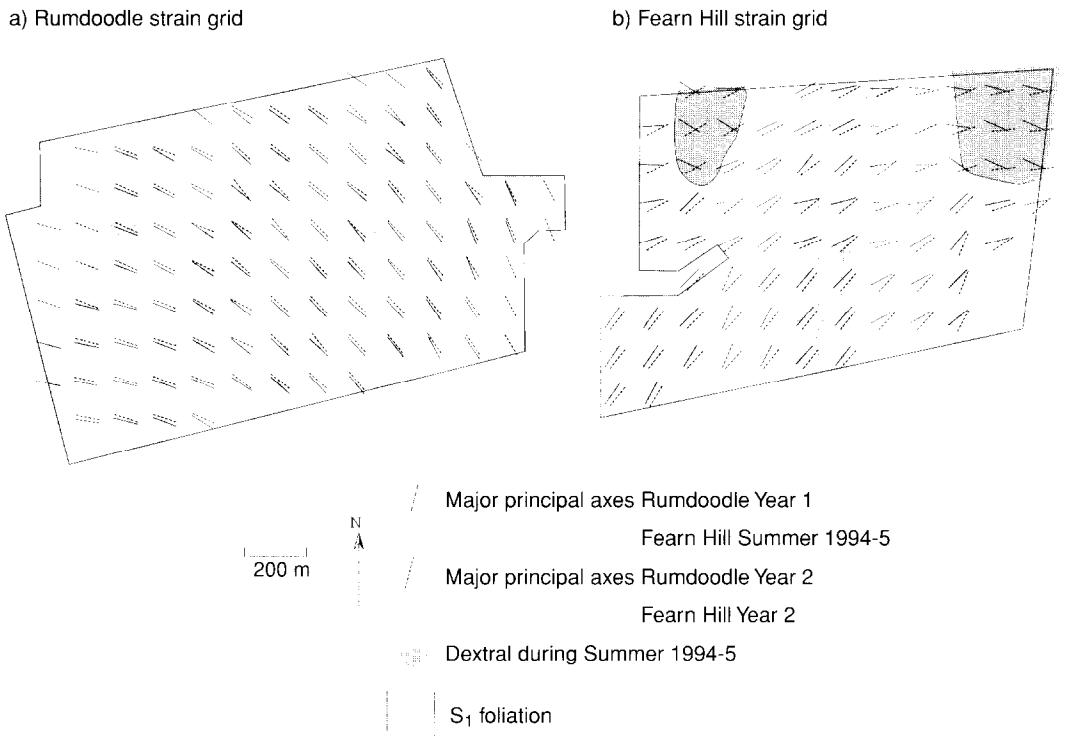

Fig. 8. Comparison of orientations of the major principal axes calculated for (a) Rumdoodle strain grid during Year 1 and Year 2 and for (b) Fearn Hill strain grid during summer 1994–5 and Year 2. The shaded areas are regions that were undergoing dextral shear during summer 1994–5 and then underwent sinistral shear for the following year.

Only sinistral shear strain was observed during the year ending in January 1996 (Fig. 8b). Shear strain rate was reduced by over a half, with values that ranged from $-0.01 \times 10^{-3}\,a^{-1}$ in the south east of the grid to $-3.22 \times 10^{-3}\,a^{-1}$ in the north west. The strain grid recorded surface area increase only in the northeast corner of the grid where the maximum dilatation was 1.001. Slight surface area decreases were distributed about the grid; however the majority of the strain grid recorded no significant surface area change.

The major principal axis of the strain ellipse rotated gradually from 030° on the west margin of the grid to 084° in the eastern margin. This rotation reflects the decreasing importance of the simple shear component toward the east. The orientation of the strain ellipses are similar to those calculated during summer 1994–5, except for those areas that underwent dextral deformation where the long axes have been rotated up to 60° anti-clockwise (Fig. 8).

DISCUSSION

Strain localisation

The nature of strain localisation can be considered by projecting a rectilinear mesh onto the ice stream (Fig. 10a). The initial orientation of this grid is considered fixed at one moment in time so that subsequent movement of the mesh describes the on going evolution of the deformation (Fig. 10b). The technique illustrates that the strain is heterogeneously distributed within the ice mass. The zones of high strain do not only occur on the margins, but also are found internally where they are interleaved with relatively rigid zones. The high strain zones display abundant brittle deformation features. Typically the brittle fractures occur at an oblique angle to the flow direction due to a significant component of shear strain acting in the plane parallel to the surface.

Comparison of strain analysis and field observations

Our field observations show that the macroscale zones of localised ductile deformation inferred from the brittle features, correlate with strain patterns obtained from analysis of strain markers. The dextral zone west of the North Masson Range, inferred from field observations, correlates with dextral shear strain recorded in the Rumdoodle strain grid, and the eastern portion of the Fang strain grid (Fig. 6). Maximum deformation occurred in the centre of the Rumdoodle grid during Year 1, suggesting that this area is the centre of a large shear zone. During Year 2, the maximum shear strain was in the northeast corner of the grid, indicating that shear strain is propagating eastward across the major shear zone. Recorded shear strain is at a minimum on the margin between the shear zone and the fracture free region to the west. The inferred zone of sinistral shear

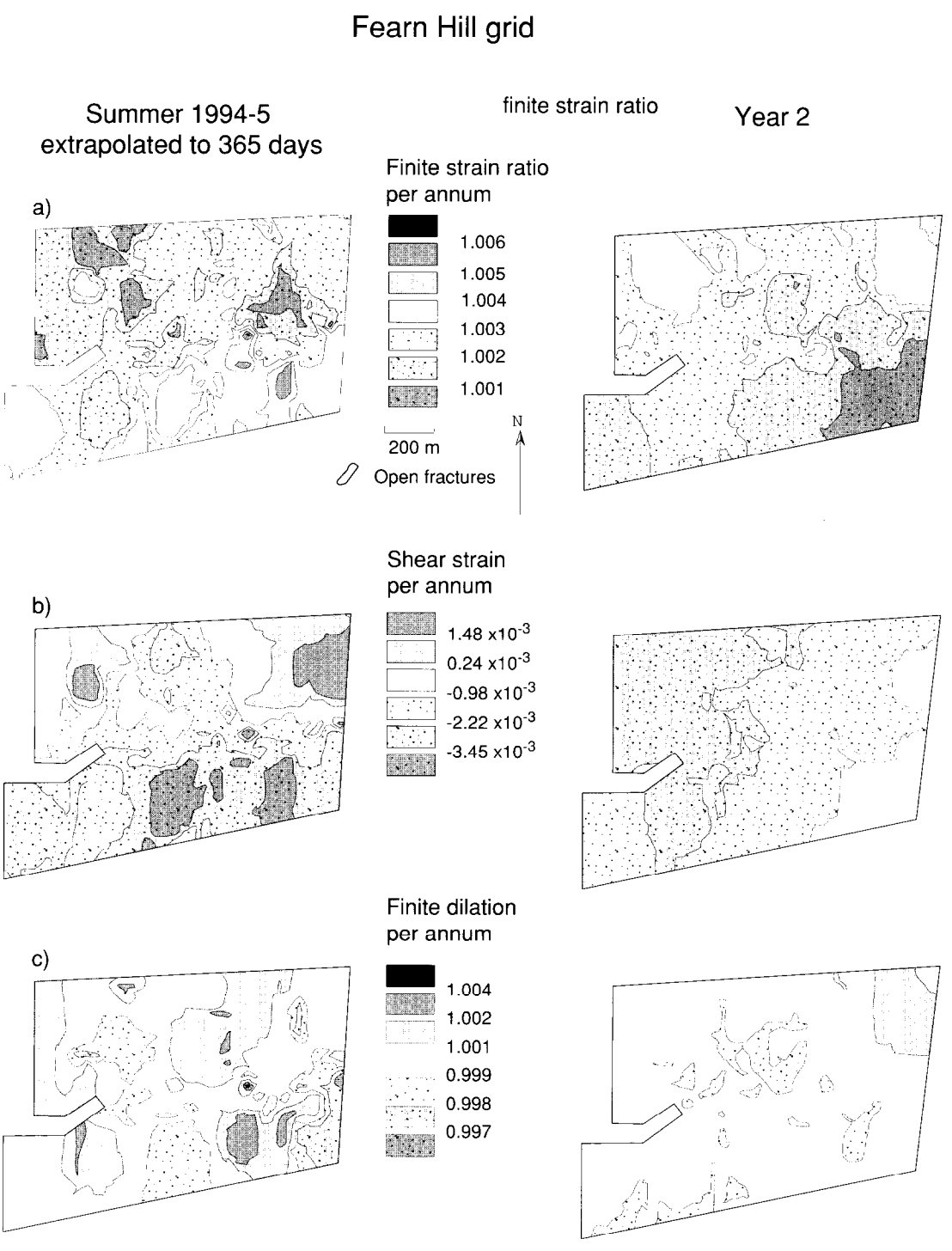

Fig. 9. Strain analysis of the Fearn Hill strain grid. The grid consists of 18 strain markers with a grid of spacing of 300 m. Results from summer 1994–5 extrapolated to 365 days (left) are compared to results from Year 2 (right). (a) A comparison of the distribution of finite strain ratio. A strong seasonal variation was recorded with strain twice as high during summer. Strain was localised into smaller discrete areas during the summer compared to the following year. (b) Distribution of shear strain rate. During Year 2 only negative values of shear strain rate were recorded, representing sinistral shear. During summer two areas in the north recorded dextral shear and shear strain rate was twice as high. (c) Dilatation rate: values greater than 1 represent regions of increasing surface area; values less than 1 represent regions of decreasing surface area. Little surface area change was recorded in Year 2 and only area increase occurred in the NE corner correlating with the open fractures observed.

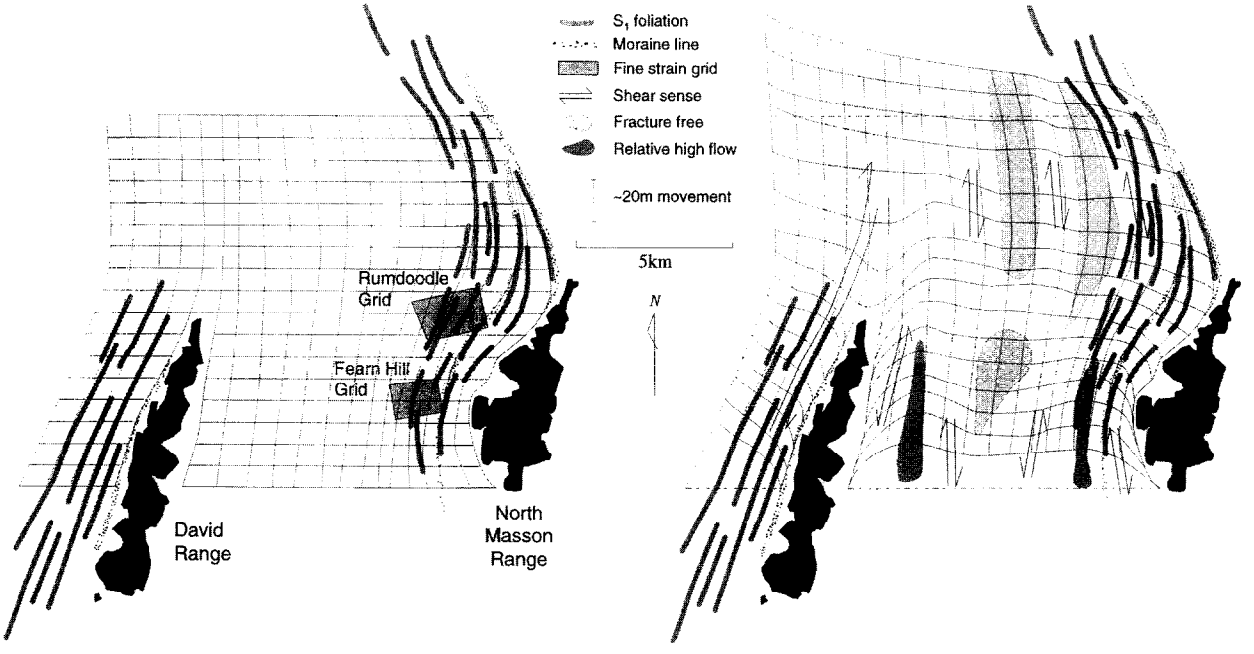

Fig. 10. A qualitative rectilinear mesh summarising the nature of deformation in Ice Stream B. (a) The mesh at the beginning of the survey (December 1993). Curved lines are parallel to flow. The S_1 foliation and position of the Rumdoodle and Fearn Hill strain grids are also shown. (b) The deformed mesh at the end of the survey (January 1996). Deformation has been concentrated on the margins of the ice stream and within several internal shear zones.

propagating through the western section of the Fang grid also correlates with the orientation of the strain ellipse calculated from survey data. The region of insignificant shear strain between these two shear zones correlates with a zone of relative high flow inferred from field data (Fig. 6a). The major axes of the strain ellipse are perpendicular to the flow direction, indicating that the region was undergoing pure shear in a compressional flow regime. The deceleration of the ice as it moves north produces this compression.

The presence and orientation of open fractures (Fig. 4a) correlate with the strain calculated from the strain grids. The development of two new fracture zones on the eastern margin of the Rumdoodle grid reflects eastward propagation of strain during Year 2 (Fig. 7). The progressive localisation of strain into sub-parallel zones probably represents a strain accommodation phenomenon in which deformation is partitioned into narrow zones undergoing compression, separated by lower strain zones that preserve earlier fabric elements. The latter areas would then be subject to a different mode of deformation; in the case of the ice mass this would provide the means of initiating an episode of brittle deformation.

The zones of active fracture initiation were confined to regions that underwent surface area increases, as modelled from the strain marker distribution (Figs 6, 7 & 9), and correspond to extensional zones that are located between the zones of compression. The broad zone of active fracturing recognised in the Rumdoodle grid (Fig. 7) during Year 1, correlated with a region that underwent surface area increase. This broad zone of open fractures separated into two discrete zones during Year 2, in response to the propagation of a region undergoing active surface area decrease into the area that had previously contained a zone with open fractures (Fig. 7). Active fractures within the Fearn Hill grid were also confined to the northeast corner, which was the only region to experience a surface area increase (Fig. 9). Crevassing and crevasse trace formation are an expression of increasing the surface area of the ice. Fracturing is therefore highly dependent on dilatation and not strain rate, making it possible for crevasses to form in relatively low strain areas. Although the local stress field distribution is important, it is the magnitude and orientation of dilatation zones that is critical in determining the distribution of crevasse areas.

For the determination of the significant strain trajectories, the ideal suite of structures used comprised arrays of en échelon fractures, offset crevasse traces and the geometric relationship between boudinaged crevasse traces. The orientation of the minimum extension directions calculated from survey data are parallel to the orientation of open fractures throughout the Rumdoodle grid and the NE corner of the Fearn Hill grid. Strain ellipse rotations of up to 20° have been recorded in the Rumdoodle grid and of up to 60° in the Fearn Hill grid. These rotations, as well as passive transportation, of crevasse traces are responsible for crevasse traces being offset by later fractures.

Incremental nature of strain within high strain zones

The temporal nature and location of deformation within the Rumdoodle grid varied greatly from Year 1 to Year 2 despite the bulk shear strain across the section of shear zone, monitored by the strain grid, being the same for both years. During Year 2 the strain was partitioned into small areas resulting in a large range of shear strain and strain ratio. The centre of the Rumdoodle grid, which had accommodated the largest portion of strain during Year 1, was relatively quiescent during Year 2. Instead deformation occurred in several narrow areas located in the eastern side of the strain grid during the second year.

The development of small zones of relatively high strain during the second year reflects a change in flow rate. In general the velocity of Ice Stream B decreased during the second year. However, the areas inferred by structural analysis to be relatively high flow zones increased in velocity during Year 2. This resulted in an increase in shear strain between relative high and low flow areas which expressed itself as small discrete zones of high strain.

A seasonal variation in strain has also been observed. The nature of strain localisation varied dramatically from the 1994–5 austral summer to the following year. The range of shear strain rate and finite strain ratio recorded during the summer was over twice that of the subsequent year. During summer the Fearn Hill grid recorded localised shear sense inversions. During the previous year the Fearn Hill grid recorded only sinistral deformation. These seasonal variations indicate that open fractures are only indicative of current stress conditions. The seasonal variations in strain rate may also provide a process by which strain is re-located within a major shear zone.

CONCLUSIONS

(1) The analysis of a glacial system, in the Framnes Mountains, east Antarctica, suggests that there is a distinct correlation between the localisation of ductile deformation and the distribution of brittle fractures. Similarly, changes in the pattern of fracture propagation can be correlated with progressive deformation.

(2) Zones of localised shear strain are recognised from the field analysis of brittle fractures within en échelon segments, sigmoidal shapes and overprinting relationships, it is possible to identify zones of localised shear strain. The structural features observed within these zones can be related to measured displacements of strain markers and to two dimensional strain rates calculated from these displacements.

(3) The development of brittle fractures occurs predominantly in regions that are undergoing dilatation, i.e. surface area increase.

(4) Deformation within the zones of high shear strain are incremental and temporal in nature, with the style and orientation of deformation fluctuating. Strain localisation propagates laterally within these zones resulting in localised variations between compressional deformation and extensional deformation leading to both the termination and initiation of brittle deformation.

Acknowledgements—This project would not be possible without the GPS survey data obtained in conjunction with John Dawson and Gary Butcher of the University of Melbourne, Department of Geomatics. Phil Collier from the same department, has provided many valuable suggestions regarding the conduct of the program. We would like to extend thanks to all officers and expeditioners of the Australian National Antarctic Research Expeditions (ANARE) for assistance and co-operation during the 1993–4, 1994–5 and 1995–6 field seasons with special reference to Andy Brocklesby and Nico Jones for their help obtaining ice radar data during the 1994–5 season. An anonymous referee and, in particular, Chris Talbot are thanked for their review comments on this manuscript. Logistical support by the Australian Antarctic Division, survey equipment provided Rob Kiernan and Ian Allison of the Australia Antarctic Division, by Tom Gordon of the Australian Land Information Group (AUSLIG), the Department of Geomatics of The University of Melbourne and financial support from ASAC grant number 599 are gratefully acknowledged. Thanks also to the AUSLIG for supplying additional GPS survey data and aerial photographs. Dr Brenton Worley is gratefully acknowledged for his help in preparing the final text. Also thanks to the organisers and editors associated with the Verbania meeting on Structure and Properties of High Strain Zones in Rocks, 1996.

REFERENCES

Bons, P. D., Jessell, M. W. and Passchier, C. W. (1993) The analysis of progressive deformation in rock inclusions. *Journal of Structural Geology* **15**, 403–411.

Gamond, J. F. (1987) Bridge structures as sense of displacement criteria in brittle fault zones. *Journal of Structural Geology* **9**, 609–620.

Hambrey, M. J. (1977) Foliation, minor folds and strain in glacier ice. *Tectonophysics* **39**, 397–416.

Hambrey, M. J. and Milnes, A. G. (1977) Structural geology of an alpine glacier. *Eclogae. geol. Helv.* **70**, 667–684.

Hanmer, S. and Passchier, C. (1991) *Shear Sense Indicators: a Review*. Geological Survey of Canada Paper, pp. 90–17.

Holdsworth, G. (1969) Primary transverse crevasses. *Journal of Glaciology* **8**, 107–129.

Hooke, R. Le B. and Hudleston, P. J. (1978) The origin of foliation in glaciers. *Journal of Glaciology* **20**(83), 285–299.

Hudleston, P. J. (1976) Recumbent folding in the base of the Barnes Ice Cap, Baffin Island, Northwest Territories, Canada. *Geological Society of America Bulletin* **87**, 1684–1692.

Hudleston, P. J. (1980) The development of inhomogeneous shear and crystallographic fabric in glacial ice. *Journal of Structural Geology* **2**, 189–196.

Kehle, R. O. (1964) Deformation of the Ross ice shelf, Antarctica. *Geological Society of America Bulletin* **75**, 259–286.

Kizaki, K. (1969a) Ice fabric study of the Mawson Region, east Antarctica. *Journal of Glaciology* **8**, 253–276.

Kizaki, K. (1969b) Fabric analysis of surface ice near Casey Range, east Antarctica. *Journal of Glaciology* **8**, 375–383.

Lawson, W. J., Sharp, M. J. and Hambrey, M. J. (1994) The structural geology of a surge-type glacier. *Journal of Structural Geology* **16**, 1447–1462.

Marmo, B. A. and Dawson, J. (1996) Movement and structural features observed in ice masses, Framnes Maintains, MacRobertson Land, east Antarctica. *Annals of Glaciology* **23**, 388–395.

Nye, J. F. (1952) The mechanics of glacial flow. *Journal of Glaciology* **2**, 82–93.

Paterson, W. S. B. (1994) *The Physics of Glaciers*. Elsevier Science Ltd, Oxford, England.

Schulson, E. M., Lim, P. N. and Lee, R. W. (1984) A brittle to ductile transition in ice under tension. *Philosophical Magazine* **49**, 353–363.

Sharp, M., Lawson, W. and Anderson, R. S. (1988) Tectonic processes in a surge-type glacier. *Journal of Structural Geology* **10**, 499–515.

Rist, M. A., Murrell, S. A. F. and Sammonds, P. R. (1988) Experimental results on the failure of polycrystalline ice under triaxial stress conditions. *Proceeding of the Ninth International Symposium on Ice* **1**, 118–127.

Vaughan, D. G. (1993) Relating the occurrence of crevasses to surface strain rate. *Journal of Glaciology* **39**, 255–266.

Whillians, I. M., Bolzan, J. and Shabtaie, S. (1987) Velocity of Ice Stream B and C Antarctica. *Journal of Geophysical Research* **92**, 8895–8902.